Journal of Materials Research and Technology 30 (2024) 3584–3593

Contents lists available at ScienceDirect

Journal of Materials Research and Technology

journal homepage: www.elsevier.com/locate/jmrt

Electrodeposition of nanocrystalline Ni and NiCr alloy coatings: Effects of Cr content on microhardness and wear resistance improvement

Zhan Liu [a,1], Qicheng Zhang [a,1], Xingwen Zhang [a], Zhifei Yu [a], Xiaowei Zhang [a], Qingzhong Mao [a,*], Jinfeng Nie [a,**], Yonghao Zhao [a,b,***]

[a] Nano and Heterogeneous Materials Center, School of Materials Science and Engineering, Nanjing University of Science and Technology, Nanjing, 210094, China
[b] School of Materials Science and Engineering, Hohai University, Changzhou, 213200, China

ARTICLE INFO

Keywords:
Coating
Mechanical properties
Ni-based coating
Electrodeposition
Wear properties
Grain refinement

ABSTRACT

The safety and reliability of high-speed trains depend on the brake disc. In order to improve the lifetime of brake disc and reduce the waste of resources, a coating with higher microhardness and well wear resistance is urgently needed. The effect of chromium content on the microstructure, microhardness and wear resistance of NiCr coating has been studied. Nano-crystalline Ni and NiCr coatings with superior mechanical properties were successfully prepared on the 30CrNiMo steel substrate by pulse current electrodeposition method. The inclusion of formic acid and sodium citrate was found to significantly expedite the co-deposition of Ni and Cr. The NiCr coatings with various Cr contents were prepared at current densities ranging from 200 to 300 mA/cm^2. These coatings significantly enhance microhardness and wear resistance of the substrate. The microhardness of the NiCr coating increased to 603 HV, outperforming pure Ni coating by 119 HV. Additionally, the wear rate of the NiCr coating decreased by 50% at a load of 10 N in comparison to the Ni coating. The high microhardness is attributed to grain refinement and solution strengthening. This study successfully addresses the challenges associated with electrodepositing Ni-based coatings on 30CrNiMo steel substrate and lays a theoretical foundation for the utilization of Ni-based coatings to enhance the tribological properties of materials used in high-speed train brake disc.

1. Introduction

High-speed trains prioritize safety, implementing comprehensive measures to ensure passenger security [1,2]. The safety and reliability of high-speed trains mainly depend on brake discs. Wear, oxidation, and corrosion of the brake disc surface are common problems in high-speed train systems [3–5]. The performance of brake disc surfaces is critical because they are the first components to deteriorate during braking. When brake disc wear occurs, it can shorten service life of the train, jeopardize safe operation, and cause extensive property damage and personal injuries. Enhancing surface properties through methods such as ultrasonic nanocrystal surface modification process and the application of protective coatings can significantly improve the wear resistance of brake discs [6–8]. In comparison to other surface treatment methods like sputtering, molecular beam epitaxy, evaporation and magnetron sputtering, electrodeposition distinguishes itself by enabling precise control over the properties of materials with high repeatability and accuracy [9–11]. Electrodeposition also presents a cost-effective and scalable solution for transitioning high-performance coatings from laboratory to industrial applications [12,13].

Hard chromium coating was once widely used as a protective coating due to its high hardness, wear resistance and corrosion resistance. However, their poor substrate adhesion significantly diminishes the lifespan of workpiece. Therefore, researchers have pivoted towards Ni-based alloy coatings, which adhere better to substrates and exhibit superior performance across a range of properties [14]. For example, NiTi coatings demonstrate excellent antioxidant properties and good biocompatibility, suitable for clinical applications; NiFe coating exhibit

* Corresponding author.
** Corresponding author.
*** Corresponding author. Nano and Heterogeneous Materials Center, School of Materials Science and Engineering, Nanjing University of Science and Technology, Nanjing, 210094, China.
E-mail addresses: 216116000150@njust.edu.cn (Q. Mao), niejinfeng@njust.edu.cn (J. Nie), yhzhao@njust.edu.cn (Y. Zhao).
[1] These authors contributed equally to this work.

https://doi.org/10.1016/j.jmrt.2024.04.100
Received 29 January 2024; Received in revised form 4 April 2024; Accepted 11 April 2024
Available online 12 April 2024

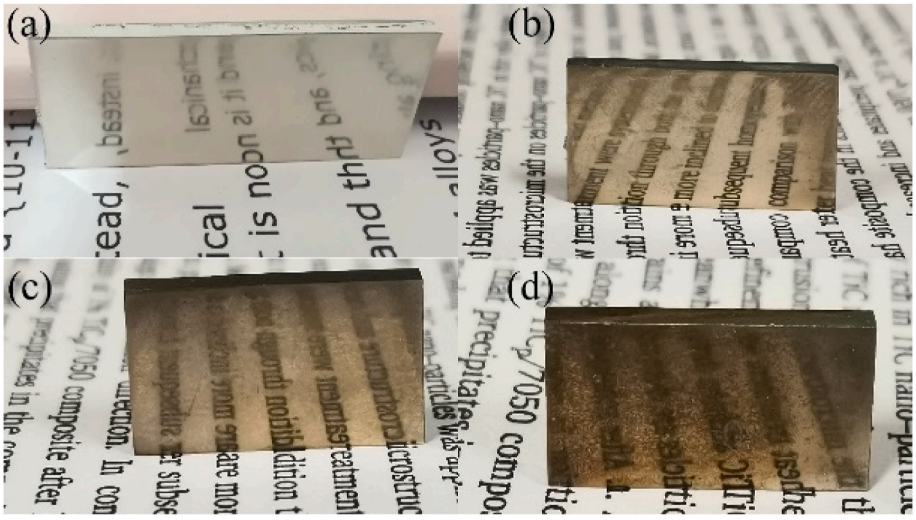

Fig. 1. Photographs of electrodeposition coatings. (a) Ni; (b) NiCr-1; (c) NiCr-2; (d) NiCr-3.

good electrocatalytic properties and can be utilized as a catalyst; NiW coatings boast high hardness and serve as an alternative to hard chromium coatings; while NiCo coatings combine high hardness with excellent electrocatalytic properties, finding applications in engine pistons, fuel cells, and other fields [15–19]. NiCr alloys, in particular, are valued for their mechanical properties and wear resistance, making them ideal for protective applications [20–22]. Electrodeposition of NiCr alloys faces challenges, mainly due to the disparate deposition potentials required for Cr and Ni co-deposition [23,24]. In previous studies, chromium anhydride has been employed as a source of hexavalent chromium ions (Cr^{6+}) for NiCr alloy electrodeposition [25,26]. However, this method suffers from several limitations. It exhibits poor dispersion and covering ability, leading to uneven deposition. Additionally, the cathodic current efficiency is extremely low, significantly prolonging the deposition time. Moreover, Cr^{6+} is highly toxic and poses significant health and environmental risks. The treatment of wastewater containing Cr^{6+} is costly and environmentally damaging, running counter to the goals of energy conservation, emission reduction, and environmental protection. Consequently, the utilization of chromium anhydride in electrodeposition solutions is gradually eliminated [27,28].

Advancements in electrodeposition processes have prompted researchers to explore trivalent chromium (Cr^{3+}) deposition solutions as an eco-friendlier alternative to Cr^{6+} [29]. One of the advantages of Cr^{3+} is its high current efficiency, meaning that a significant portion of the electrical energy is applied during electrodeposition, which ensures enhanced deposition efficiency and reduced energy consumption [30,31]. In addition, Cr^{3+} is characterized by lower toxicity and environmental pollution, producing fewer hazardous byproducts and simplifying wastewater treatment and disposal compared to Cr^{6+} [32,33]. In various Cr^{3+} electrodeposition systems, the potentials difference between Ni and Cr for co-deposition can be finely adjusted through the addition of coordination agents, and by tuning the current density, pH and temperature [34–36]. Such adjustments enable the successful co-deposition of Ni and Cr [37–39]. Zhang et al. devised an electrodeposition solution for NiCr coatings by utilizing a formate-citrate mixture with $CrCl_3$ and $NiSO_4$ [40,41]. Chen et al. developed an electrodeposition solution for NiCr coating, employing formate-acetate with $CrCl_3$ [42]. Yang et al. developed a mixed citric acid-chloride-sulfate electrodeposition solution for the fabrication of NiCr coating [43]. Zhang et al. utilized DMF as an alternative solvent to achieve crack-free NiCr coatings, given that DMF lacks hydrogen atoms [44]. However, DMF is toxic to human body, research in this area remains limited.

In spite of several researches on NiCr electrodeposition, Cu rather than steel was usually used as substrate. There are still some difficulties in NiCr coating electrodeposition on steel substrate. In this study, NiCr coatings with different contents of Cr^{3+} were prepared to improve the wear properties of the 30CrNiMo steel substrate. The impact of current density on the phase composition and properties of the NiCr coatings was investigated by utilizing formic acid and sodium citrate solution. The microhardness and friction properties of the coatings were also evaluated. In addition, the role of grain refinement and solid solution strengthening in microhardness enhancement was examined, which provides insights into the mechanisms behind the improved mechanical properties of the NiCr coatings. Based on the results of the friction tests, the protective effects of the Ni and NiCr coatings on the 30CrNiMo substrate surface were investigated. The study provides a theoretical foundation for utilizing Ni-based coatings to enhance the tribological properties of materials used in high-speed train brake discs.

2. Materials and method

2.1. Fabrication of the Ni and NiCr coatings

The high-speed train brake discs material is CrNiMo cast steel. In this study, 30CrNiMo steel with dimensions of $10 \times 30 \times 2$ mm^3 was used as the substrate. Prior to electrodeposition experiment, the substrate was

Table 1
Bath composition and deposition conditions of electrodeposition used for Ni and NiCr alloy co-electrodeposition.

	Pure Ni	NiCr
$NiCl_2{\cdot}6H_2O$	40 g/l	30 g/l
$Ni(SO_3NH_2)_2$	300 g/l	/
$CrCl_3{\cdot}6H_2O$	/	100 g/l
$C_6H_5Na_3O_7$	/	80 g/l
H_3BO_3	40 g/l	40 g/l
$C_7H_5NO_3S$	0.6 g/l	/
$C_{12}H_{25}SO_4Na$	0.6 g/l	0.1 g/l
HCOOH	/	46 g/l
NaBr	/	15 g/l
Anode	Pure nickel plate	Pure nickel plate
Current density	100 mA/cm^2	200–300 mA/cm^2
Temperature	50 °C	30 °C
Time	1 h	1 h
pH	4	3.5
Interelectrode gap	40 mm	40 mm
Stirring speed	30 r/min	30 r/min
Pulse frequency	10 Hz	10 Hz
Duty cycle	0.5	0.5

mechanically grounded using 320–2000 grit standard abrasive papers, cleaned using a 10% (wt.%) NaOH aqueous solution at 80 °C for 10 min, followed by a 10% HCl solution immersion for 16 s to remove oxidation layer to improve adhesion. The clean substrate was partially covered with Teflon tape, leaving an area of 1 cm × 3 cm exposed. The electrodeposition of pure Ni and NiCr coatings was executed using double pulse power supply (SOYI-VA-DM, China). The solution composition selection process is shown in supplementary materials (Table S1). The electrodeposition coatings containing lower defects (pits and holes) with smooth surface morphologies were chosen in this study (Fig. S1). In addition, the deposition rate of Cr significantly depends on the applied current density, whereas the electrodeposition rate of Nickel remains unaffected [45]. Consequently, three current densities (200, 250 and 300 mA/cm^2) were selected to produce NiCr coatings with different Cr contents (according to Table S1), respectively named NiCr-1, NiCr-2 and NiCr-3, and the pure Ni coating was named Ni. The electrodeposition bath temperature was maintained by a digital heating circulating water bath (DF-101S, China). Additionally, stirring is used to ensure a constant ion concentration in the electrodeposition solution. $NiCl_2$-$6H_2O$ and $CrCl_3$-$6H_2O$ served as ion sources of Ni^{2+} and Cr^{3+}. H_3BO_3 was used as a buffer to stabilize the pH. $C_{12}H_{25}SO_4Na$ was used as a surfactant to improve the brightness and reduce grain size. HCOOH and $C_6H_5Na_3O_7$ were utilized as complexing agents to minimize the potential difference between Ni^{2+} and Cr^{3+} to promote the co-deposition of Ni and Cr. NaBr was used as a conductive salt to improve the conductivity of solution. A chloride bath was chosen for electrodeposition due to its wide current density adaptability, lower voltage requirement, high conductivity, and absence of sulphur co-deposition, resulting in smaller grain size [46]. Detailed experimental parameters are provided in Table 1. Fig. 1 shows surface photographs of Ni and NiCr electrodeposited coatings. These photographs confirm the successful electrodeposition of pure Ni and NiCr alloy coatings on the 30NiCrMo steel substrate. The Ni coating (Fig. 1a) showcases a tangible mirror-like effect, indicating a high degree of surface smoothness and reflectivity. In contrast, the NiCr coatings (Fig. 1b–d) exhibits a dull yellowish mirror-like effect with minor surface protrusions. The presence of the NiCr coating suggests that they may have a slightly rougher surface compared to Ni coating. As the Cr content increased, the electrodeposited coatings appeared progressively dimmer. The findings suggest a trade-off between increasing Cr content and the overall roughness of the coatings, while still maintaining their reflective capability to some extent.

2.2. Current efficiency testing

The cathode current efficiency (η) was calculated according to Faraday law [16,47]:

$$\eta = \frac{\Delta m \bullet F}{I_{average} \bullet t} \sum \frac{w_i \bullet n_i}{M_i} \times 100\% \quad (1)$$

where Δm (g) is the mass increase of the cathode after electrodeposition. Where $I_{average}$ (A/cm^2) is the average current density used during electrodeposition, $I_{average} = I_{peak} \times \gamma$, γ is duty cycle. Where t (s) is electrodeposition time, w_i is the mass fraction of each metal (Ni or Cr), n_i is the number of electrons gained by each metal during the electrodeposition, F is Faraday's constant (96845 C mol^{-1}), and M_i is the molecular weight of each metal (g· mol^{-1}).

2.3. Microstructure characterization

The microstructure and elemental composition of Ni and NiCr electrodeposited specimens were characterized by a scanning electron microscope (SEM, FEI Quant 250F, USA) equipped with an energy dispersive spectroscopy (EDS). The phase composition was analyzed by a Bruer D8 X-ray diffractometer. XRD patterns were recorded between 20° and 100° with a scan rate of 2° min^{-1}. The morphology of the wear scars was characterized by a laser confocal 3D profiler (SM-1000, Applied Scientific Instrumentation, USA). The wear rate was calculated according to the wear rate formula K $[mm^3/Nm] = V/(P \times S)$, where V represent the wear volume, P represents the applied load, and S denotes the total sliding distance.

2.4. Mechanical properties and frictional behavior test

The Vickers microhardness was measured utilizing an HMV-G 21DT under an applied load of 25 mN and a duration time of 15 s. At least fifteen points were measured for each specimen. The friction tests at room temperature were carried on a tribometer (UMT-II, Germany). The sliding stroke and speed was set at 1 mm and 4 mm/s. Normal loads of 2 N and 10 N were applied in the wear tests. The Φ6 mm Al_2O_3 ball with a microhardness of 1650 HV is selected as counterbody.

3. Results

3.1. Microscopic characters of electrodeposited coatings

The surface morphologies of the electrodeposited coatings are shown in Fig. 2. The Ni coating exhibits a smooth and defect-free surface (Fig. 2a and b). In contrast, the NiCr coating shows a characteristic pattern of cracks that resemble a tortoise shell. These cracks are observed to divide the coating into regions where small cracks do not reappear. These cracks are typical of hard chromium coating and suggest microstructural changes and potential stress concentrations within the coating. In the process of NiCr electrodeposition, a large amount of hydrogen was generated mainly because of the discharge of hydrogen ions on the cathode, chromium hydrides (CrH and/or CrH_2) are formed, resulting in the accumulation of internal stress in the coating [44]. As hydride concentration within the grains increases, so does the internal stress. When the stress concentration becomes too high, it can exceed the mechanical strength of the coating, leading to crack formation [48,49].

We calculated the number of intersection points per unit line to quantify the crack density [50]. The results indicate that crack density escalates with an increase in Cr content (from 5.99 × 10^{-3} μm^{-1} to 2.23 × 10^{-2} μm^{-1}). Notably, despite variations in Cr content, the width of these cracks remains consistent (100–400 nm). This finding suggests that the width of the cracks is not directly correlated with the Cr content in the coatings. Notably, in Fig. 2e-g, nodular deposits can be seen within the NiCr coatings. Similar nodular deposits are often observed on the surface of Cr coatings [36]. Fig. S2 shows further details on the particles' morphology.

Fig. 3 displays the cross-section views of the Ni and NiCr coatings. The average thickness of each coating is about 184 μm, 4.5 μm, 4.5 μm, and 18.1 μm, respectively. The NiCr coatings are thinner than the Ni coating, attributable to the lower co-deposition efficiency of NiCr compared to that of Ni electrodeposition. In Fig. 3b, 3c and 3d, inherent cracks can be observed in the coatings. These cracks also present in the pure Cr coatings [32]. Notably, these inherent cracks align with those observed on the surface of the coatings in Fig. 2. These penetration cracks are sites of severe stress concentration, leading to diminished corrosion resistance [51].

Fig. 4 illustrates the surface morphology and corresponding EDS mapping results of each coating, including element distribution images and mass percentage. The EDS mappings indicate uniform distribution of Ni and Cr ions throughout the coatings. According to the mass percentage given by EDS analysis, the coatings can be identified as follows: Ni_{100}, $Ni_{97.3}Cr_{2.7}$, $Ni_{96.6}Cr_{3.4}$ and $Ni_{95.6}Cr_{4.4}$. The Cr content of coating is directly related to the pulse current density, assuming other conditions remain constant. As the current density increases, the electric energy used for metal deposition increases, the cathode polarization easier, and the deposition speed of Cr^{3+} increases [35]. The cathode current efficiency of each coating is 84.6%, 45.2%, 44.4%, 47.1%, according to equation (1). It can be observed that Cr^{3+} reduces cathode current

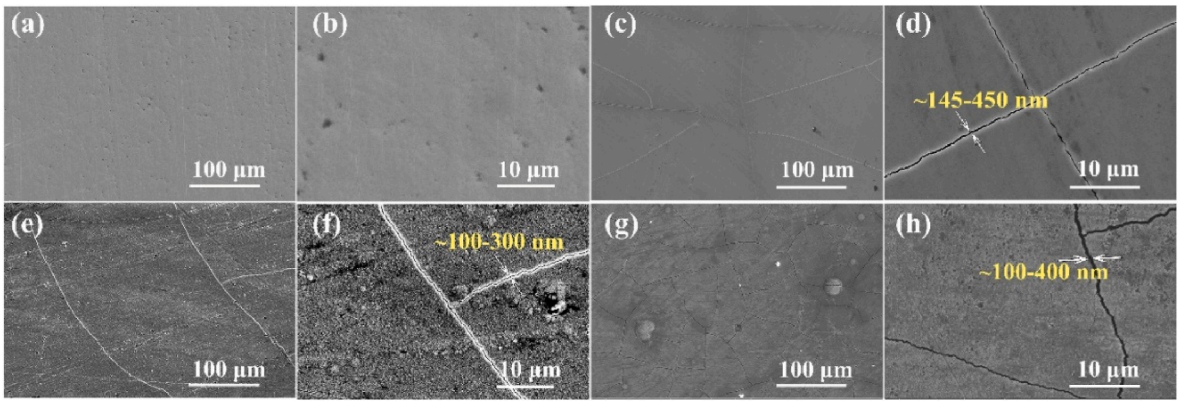

Fig. 2. SEM images of electrodeposition coatings: (a, b) Ni; (c, d) NiCr-1; (e, f) NiCr-2; (g, h) NiCr-3.

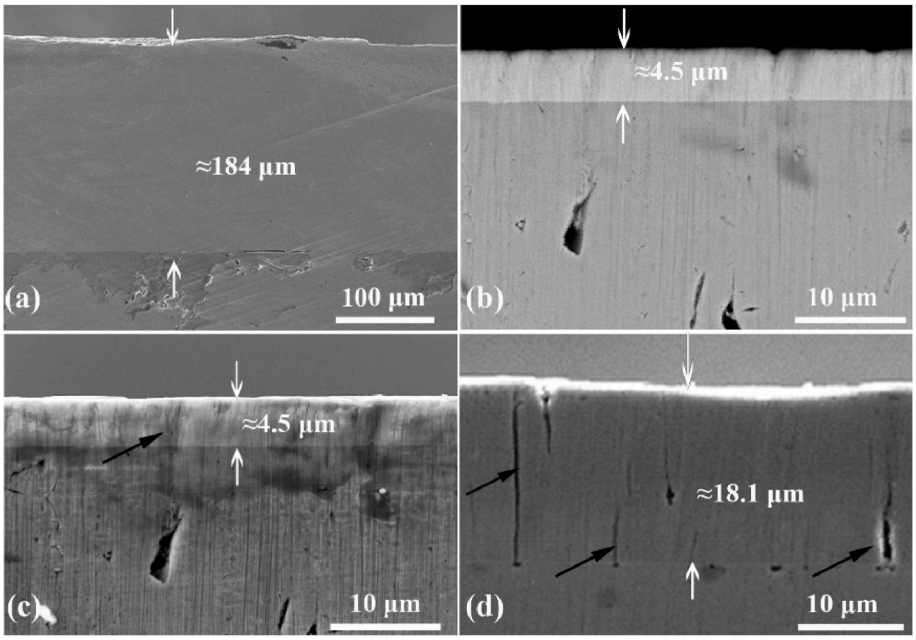

Fig. 3. Cross-sectional micrograph for electrodeposition coatings: (a) Ni; (b) NiCr-1; (c) NiCr-2; (d) NiCr-3.

efficiency due to the more challenging electrodepositing process compared to Ni^{2+}. The higher current density, the higher cathode current efficiency and the higher Cr content in coatings.

The XRD patterns indicate that the NiCr coatings contain only the FCC phase (Fig. 5), indexed by the (111), (200), (220), (311) and (222) peaks, and no typical peak of the BCC phase (Cr) appears in NiCr coatings. The (111) plane shows the highest diffraction intensity from the XRD patterns, indicating it as the preferential direction in the coatings. The (220) plane, showing the lowest diffraction intensity, is not clearly identifiable. According to the NiCr binary phase diagram, the Ni-rich FCC phase has a very high (up to 50 at.% at 1345 °C) solubility of Cr, which still remains comparatively high at 590 °C with about 32 at.% [52]. The XRD analysis confirms that Cr atoms in the NiCr alloy coating dissolve into the Ni matrix, forming a Ni-Cr solid solution. Furthermore, the lattice parameter of the NiCr coatings is measured at 3.53 Å. The fact that all three NiCr coatings have the same lattice parameter value suggests that the crystal structure remains consistent throughout the different coatings. Additionally, the pattern of the coatings (Fig. 5) displays a broad (111) peak due to the grain refinement.

3.2. Friction and microhardness tests for electrodeposited coatings

The microhardness of the substrate, as-deposited Ni, and as-deposited NiCr are shown in Fig. 6. The microhardness of the substrate, Ni, NiCr-1, NiCr-2, NiCr-3 is 173 ± 4 HV, 484 ± 14 HV, 575 ± 33 HV, 590 ± 31 HV, 603 ± 26 HV, respectively. The inset is morphology of coatings after microhardness test. The length of diagonal of NiCr coatings is approximately 9 μm and the depth is about 1.3 μm. The depth of indentation is shallower than the thickness of NiCr coatings. The results indicate that this enhancement in microhardness is attributed to the presence of the deposited materials (Ni or NiCr) on the substrate surface. Specifically, the incorporation of Cr into the Ni matrix results in solid solution strengthening, thereby increased the microhardness. The correlation between current density, Cr content, and the microhardness of the coatings will be discussed later.

At lower current densities during the electrodeposition process, the co-deposition efficiency of Ni and Cr is relatively low, resulting in thinner NiCr coatings (Fig. 3). Therefore, only NiCr coating with a thickness of 18 μm was selected for the friction test. Fig. 7a shows the variation in the coefficients of friction (COF) with sliding time for different coatings under 2 N and 10 N normal loads. At the initial stage of friction, the COF of all three samples rapidly increases and exhibits

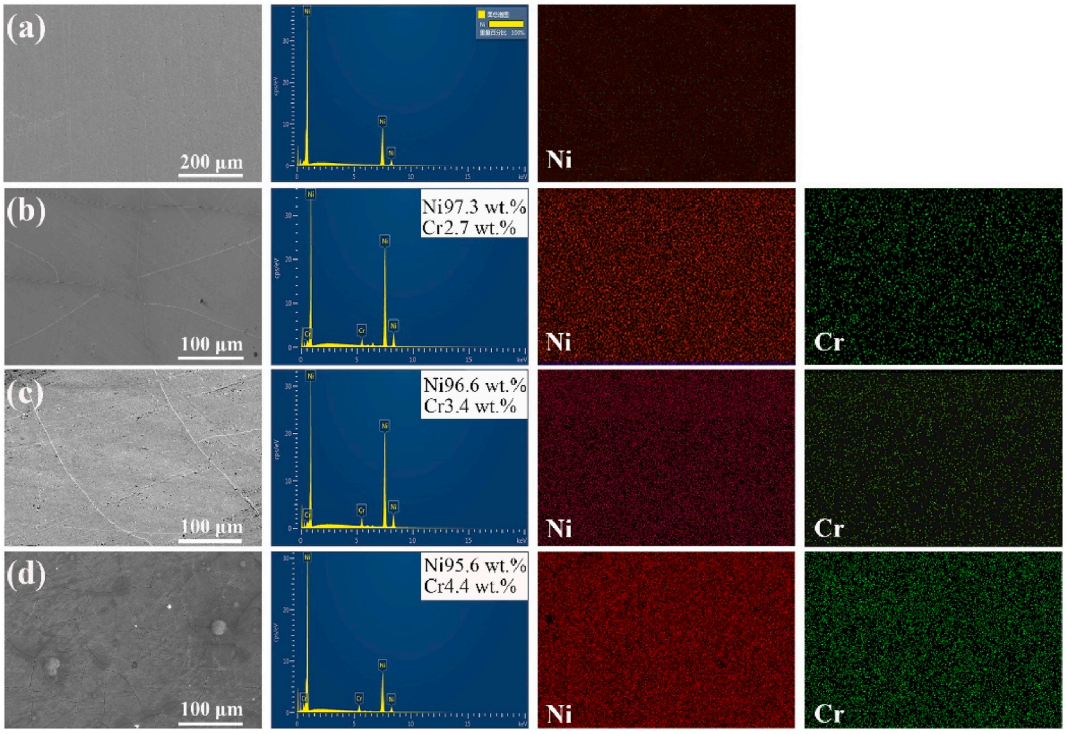

Fig. 4. SEM micrographs and EDS mappings of electrodeposition coatings: (a) Pure Ni; (b) NiCr-1; (c) NiCr-2; (d) NiCr-3.

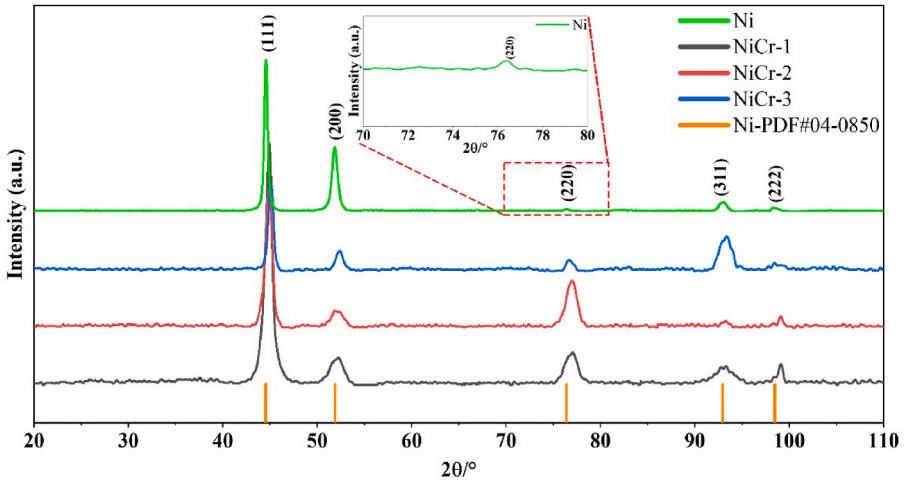

Fig. 5. X-ray diffraction patterns of electrodeposition coatings.

significant fluctuation. Subsequently, the COF of the Ni coating gradually stabilizes. As the normal load increases from 2 N to 10 N, the COF of both Ni and NiCr coatings decreases. The COF of the NiCr coating under the 10 N load shows considerable fluctuation, attributed to the presence of inherent surface cracks. During the sliding process, these cracks will experience stress concentrations, leading to fracture or separation of the coating from the substrate and causing larger variations in the COF. In contrast, the COF of substrate increases with normal load. Then the average COF of all samples was counted. The results are shown in Fig. 7b, the average COF of Ni coating is 0.235 and 0.228 under the normal loads of 2 N and 10 N, respectively. The average COF of NiCr coating is 0.306 and 0.254 under normal loads of 2 N and 10 N. In general, the COF of all samples indicates that the substrate and the coatings exhibit distinct frictional behavior.

Fig. 8 shows the 3D profiles of wear surface morphologies for the substrate and the coatings. It is observed that both the depth and width of the wear tracks increase with increasing normal load, exhibit an increase. The shallow and narrow wear tracks of Ni coating (2 N) and NiCr coating (2 N and 10 N) correspond to their low specific COFs. It is noted that there is the obvious pile-up of wear debris on the edge of the substrate, but no obvious pile-up on the coatings. Analyzing the 3D profile of the wear tracks enables the measurement of cross-sectional areas, which can then be used to calculate the wear rate.

The depth of the wear tracks and the wear rates are plotted in Fig. 9a and b. Under the normal load of 2 N, the wear track depths of all samples are comparable, measuring around 2 μm. The substrate exhibits the highest depth of 5 μm under the normal load of 10 N. While the depth of the wear tracks of Ni and NiCr coatings remains relatively unchanged and stays around 2 μm. From Fig. 9b, it is apparent that the increasing normal load within the sample leads to an increase in the V_{wear}.

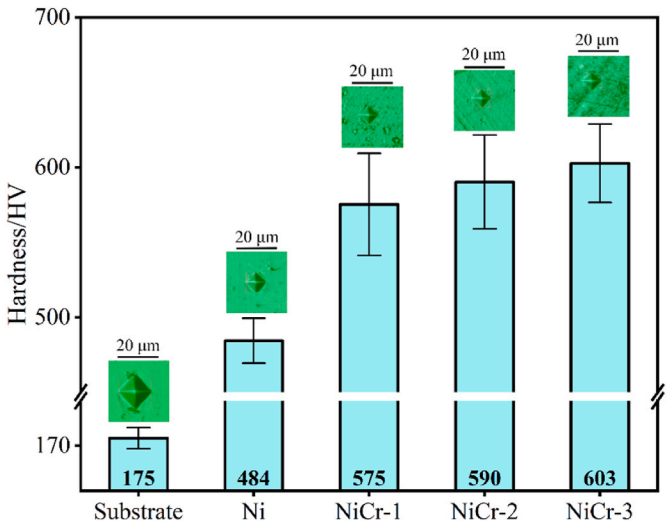

Fig. 6. Microhardness of substrate and electrodeposition coatings.

Comparing the three samples, it is evident that the substrate exhibits the highest V_{wear} and wear rate. Notably, the wear rates for the Ni and NiCr coatings are relatively consistent under varying loads. According to Archard's equation, higher microhardness generally indicates better wear resistance. Since the microhardness of the Ni and NiCr coatings is greater than that of the substrate (Fig. 6), the coatings exhibit better wear resistance.

Fig. 10 shows the wear surfaces of both the substrate and the coatings. Fig. 10a shows that after friction under the normal load of 2 N, the wear tracks of the substrate display the morphologies including peeling and abundant shallow grooves along the sliding direction (SD) accompanied with some vertical cracks. In addition, the width of the wear tracks is only 193 μm. As the load increases to 10 N, the wear track width doubles to 430 μm (Fig. 10b). In addition, the crack density increases with the incremental load. The observation of stratification in the wear tracks suggests that the primary wear mechanism of the substrate is delamination wear.

The width of the wear tracks of the Ni coating measures 177 μm and 355 μm under the normal load of 2 N and 10 N. From Fig. 10c and d, it can be observed that the microscopic morphology of wear tracks of the Ni coating under different loads exhibits similar characteristics, indicating an abrasive wear mechanism.

Fig. 10e and f shows the morphologies of the wear tracks of NiCr coatings under the normal load of 2 N and 10 N, respectively. The width of the wear tracks of the NiCr coating measures 103 μm and 277 μm under the normal load of 2 N and 10 N. The wear surfaces of NiCr coating at different loads show grooves and cracks. However, Fig. 10e1 and 10f1 provide a local magnification area of the wear track, it is observed that apart from the existing inherent cracks in NiCr coating, new micro-cracks appear along the periphery of the inherent cracks after friction. It is clear that abrasive wear is the main mechanism and the corresponding sub mechanisms are micro-cracks.

Fig. 11 shows the EDS mappings of the wear surface after friction under the normal load of 2 N and 10 N. In Fig. 11, the wear surface could be divided into the bright and dark regions which are recognized as the nonoxidation and oxidation zones (see the EDS mappings of oxygen element). Some thin plate-like peels along the SD could be found in the oxidation zones. Additionally, the areas experiencing deformation at the edges of the wear tracks may undergo a certain degree of oxidation before spalling occurs. Notably, there exists some scratches on the NiCr coating under 2 N load (Fig. 11e). An enrichment of oxygen and aluminum is observed on the NiCr coating. The enrichment is speculated to be the residue of the Al_2O_3 counterbody. The distribution of other elements of all samples remained relatively uniform throughout the wear process.

In general, the NiCr coating including higher COF and lower wear tate compared to 30CrNiMo steel under identical conditions. The higher COF means the system can stop the strain at shorter time and distance, the lower wear rate indicates longer serve life. The larger the current density, the higher the crack density, the smaller the grain size, the higher the microhardness, which lead to better wear resistance. The electrodeposition baths for the NiCr coating utilized a borader range of current densities than those for the Ni coating. Moreover, the presence of solid Cr atoms bolsters the microhardness and wear resistance of the NiCr coating. The NiCr coating does not easily occur to dislocation, deformation and delamination, but easily occurs to plough during friction test. According to Archard's equation, higher microhardness generally indicates better wear resistance. In this study, the NiCr coating exhibits superior microhardness compared to both the Ni coating and 30CrNiMo steel. The tribomechanical properties of the Ni coating and 30CrNiMo steel was increased by the included Cr element. The crack density has no significant effect on the performance of NiCr coatings.

4. Discussion

Occasionally, wear is not in accordance with the friction. The wear rate of NiCr coating is lower than that of Ni coating, yet the COF of NiCr coating is higher. A plausible explanation for this phenomenon is the

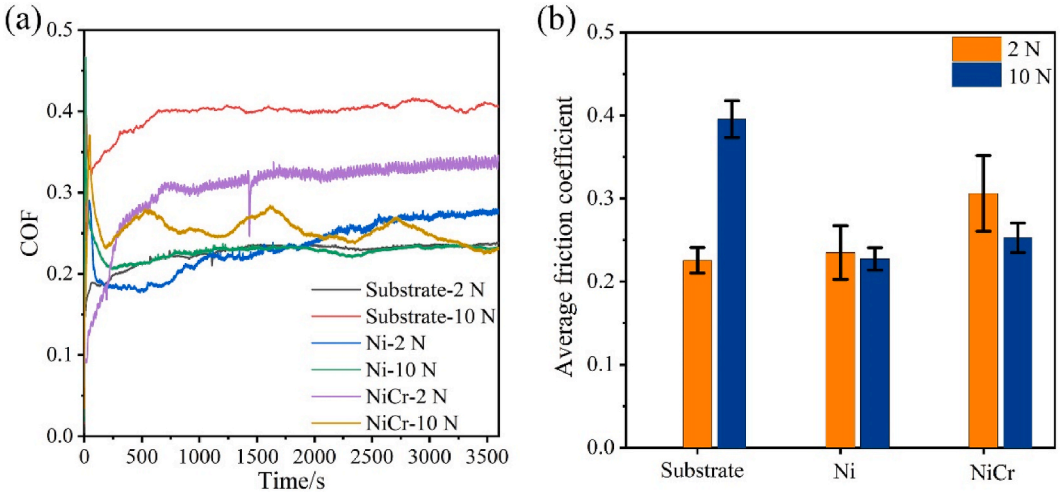

Fig. 7. (a) Variation of COF with times under different normal loads; (b) the average COF value of substrate and coatings under different normal loads.

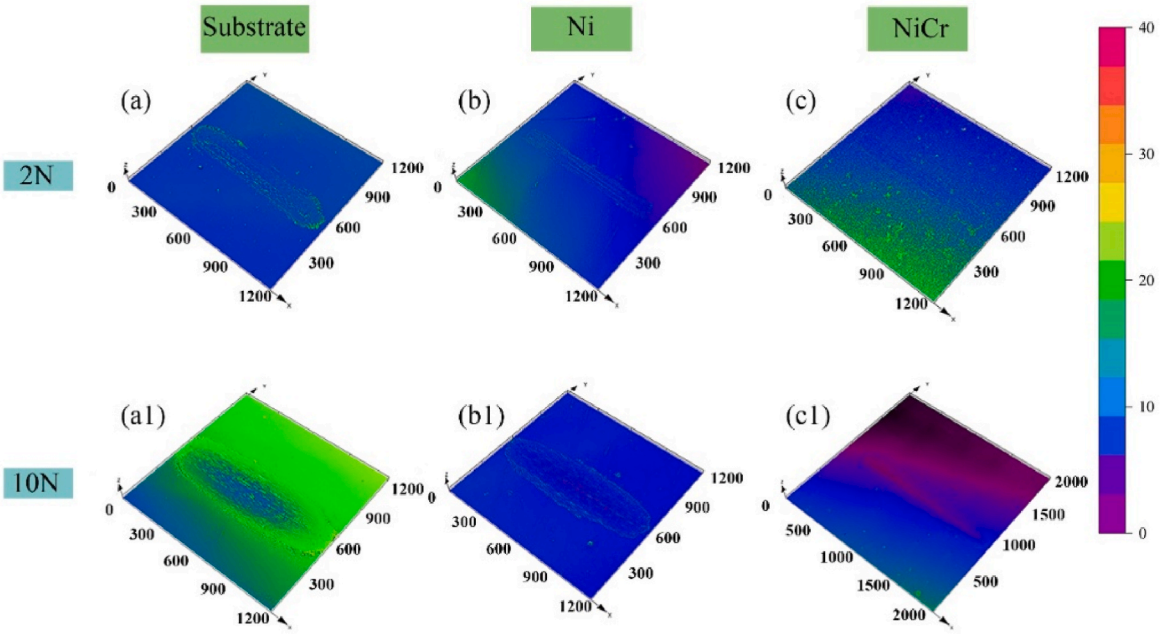

Fig. 8. The 3-D profiles for wear surface morphologies of the substrate and coatings: (a, a1) Substrate; (b, b1) Ni; (c, c1) NiCr-3.

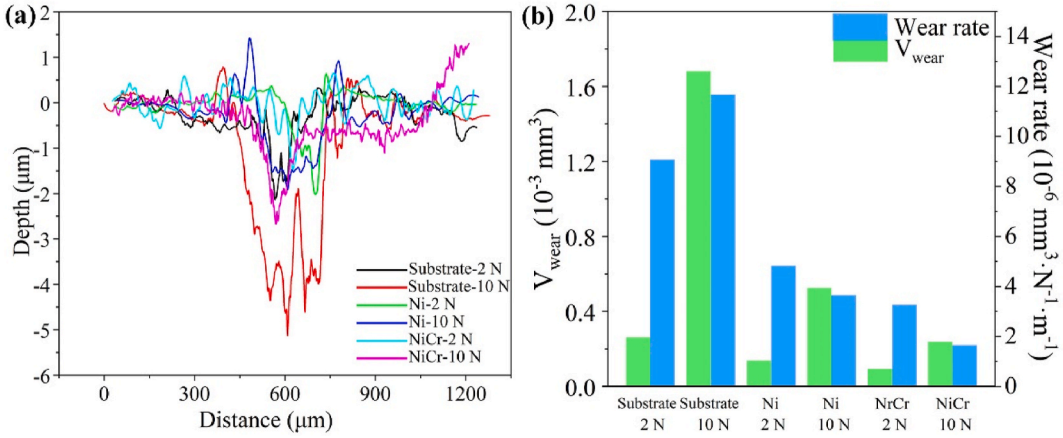

Fig. 9. (a) Cross-sectional profiles of wear surfaces under different normal loads; (b) wear volume and wear rate under different normal loads.

greater resistance of NiCr coating to plastic deformation. According to Archard's equation, higher microhardness generally indicates better wear resistance. The increase in COF of the NiCr coating may result from unstable Al_2O_3-to-NiCr contact due to microcracks.

It is well-established that grain refinement and the pinning effect of solid solution atoms significantly improve the mechanical properties of metals. These two strengthening mechanisms also enhance the properties of electrodeposition coatings. In the context of alloy electrodeposition, elevated current densities thermodynamically promote grain nucleation, leading to the formation of submicron or even nanocrystalline structures [53]. Herein, the grain sizes of different electrodeposition coatings were calculated by Scherrer's formula [54]. The grain size of Ni, NiCr-1, NiCr-2, NiCr-3 coating are 15 nm, 10 nm, 11 nm, 10 nm, respectively. Based on EDS and XRD analysis results, none BCC chromium phase was formed in the NiCr coatings, indicating that the Cr atoms are well solid-solved in the Ni matrix. Consequently, two strengthening mechanisms contribute to the microhardness of NiCr coatings, as shown below [55,56]:

$$H = H_0 + \Delta\sigma_{ss} + \Delta\sigma_{GB} \tag{2}$$

where H is the microhardness, H_0 is the microhardness of Ni single crystal; $\Delta\sigma_{ss}$ is solid solution strengthening; $\Delta\sigma_{GB}$ is grain refine strengthening.

The dissolved of Cr atoms causes lattice distortion and inhibits the dislocation movement, which can be expressed as follows:

$$\Delta\sigma_{ss} = HC^n \tag{3}$$

where C is the concentration of solid solution Cr in Ni matrix, which was obtained by the averaging of various EDS mapping analyses in NiCr coatings (as shown in Fig. 4); H and n are constants. According to Matsui et al., n is 2/3 [57]. The calculated $\Delta\sigma_{ss}$ for NiCr coatings with different Cr contents are listed in Fig. 12a. Considering the contribution of grain refinement, smaller grains result in an increased density of grain boundaries, which effectively inhibit dislocation movement during the deformation process. The contribution of grain refinement to

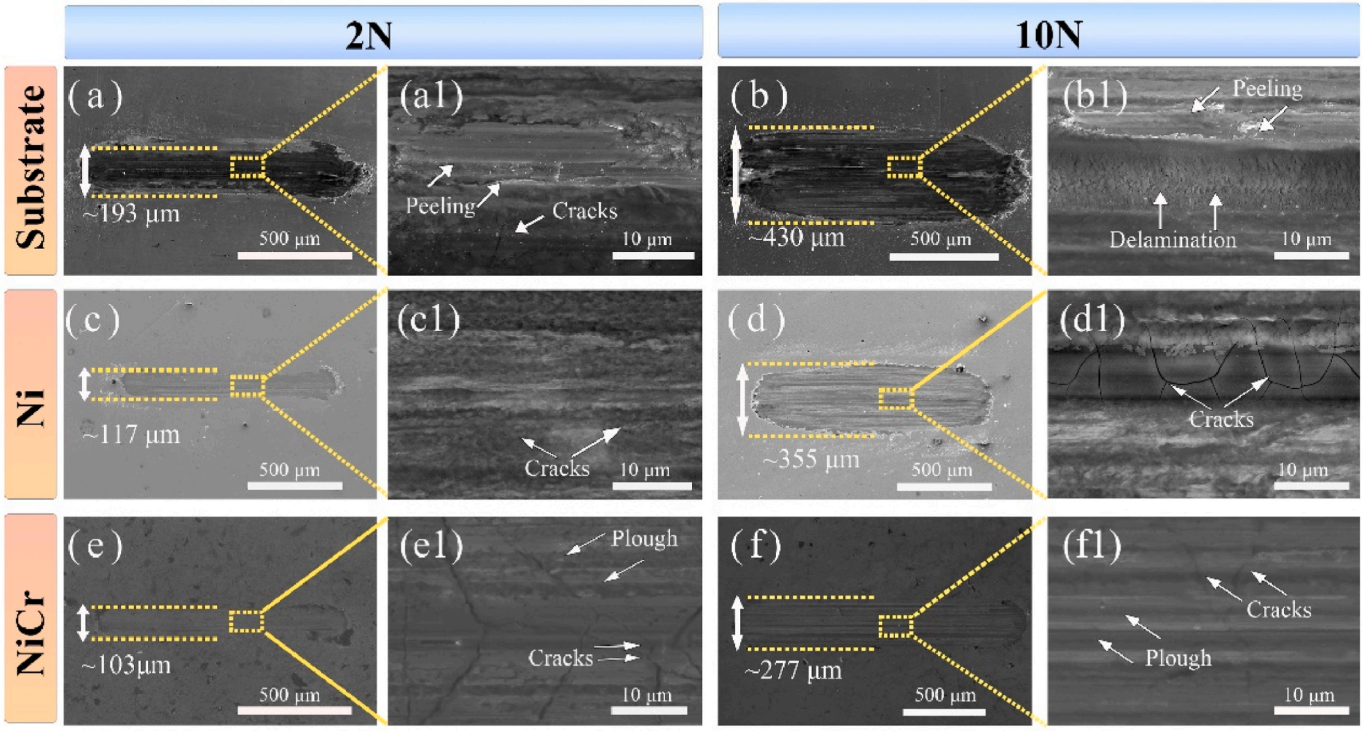

Fig. 10. SEM micrographs for the wear surface: (a-b1) substrate; (c-d1) Ni coating; (e-f1) NiCr coating under different normal loads.

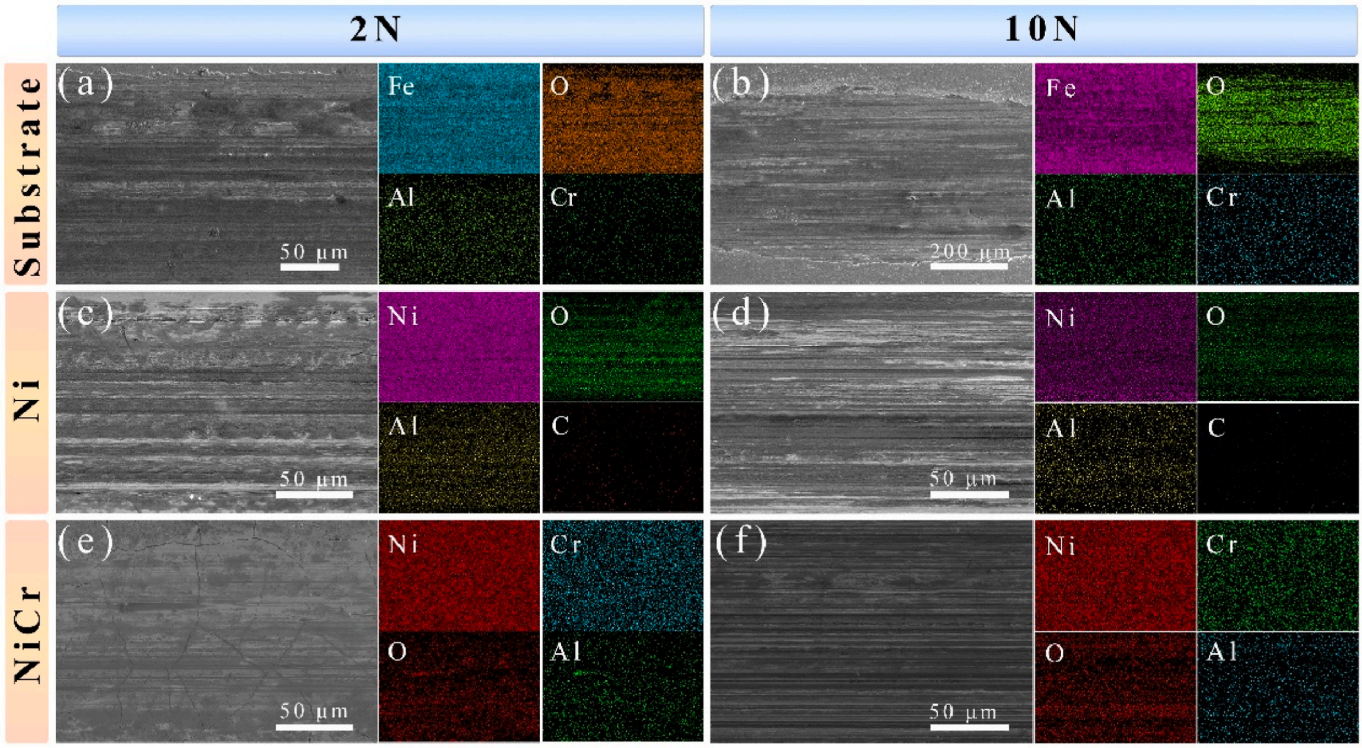

Fig. 11. SEM micrographs and EDS mappings of wear surface of (a, b) substrate; (c, d) Ni coating and (e, f) NiCr coating under different normal loads.

microhardness can be described by the Hall-Petch formula [58]:

$$\Delta\sigma_{GB} = k_{H-P} d^{-\frac{1}{2}} \quad (4)$$

where $k_{H\text{-}P}$ is the Hall-Petch slope; d is the grain size. A linear fit was computed for all data in Fig. 12b, the line shown to intersect the data gives the slope k_{H-P} = 1622 HV nm$^{1/2}$. The calculated theoretical microhardness of coatings corresponding to formula (2) are shown in Fig. 12c. Notably, except for NiCr-1, there is a close alignment between the experimental and theoretical microhardness of NiCr coatings.

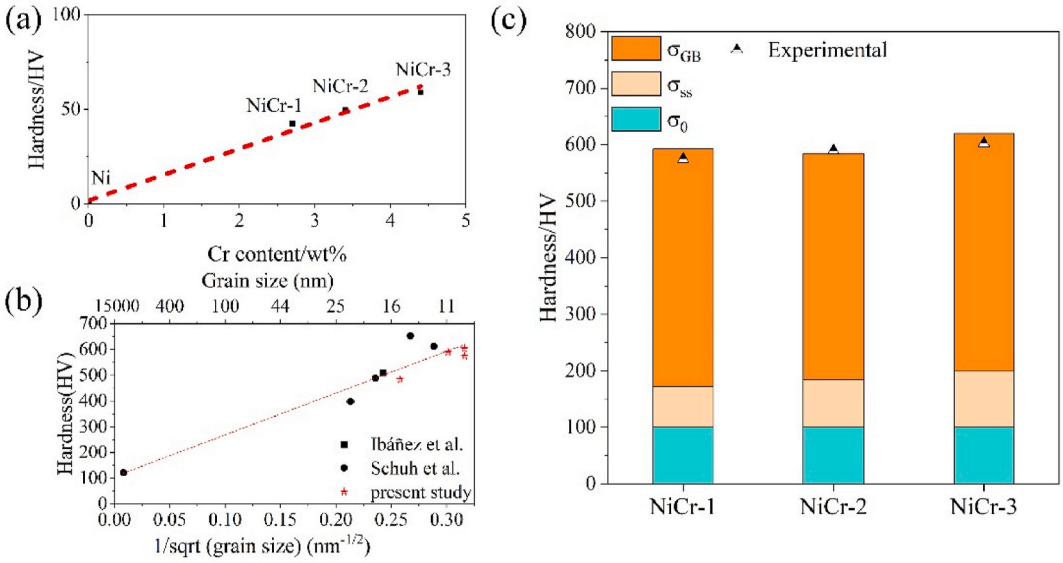

Fig. 12. (a) The contribution of solid solution strengthening on microhardness; (b) The contribution of grain refinement strengthening, the present results are compared with those of Schuh et al. [59] and Ibáñez et al. [60], who used electrodeposition to produce nickel specimens; (c) Comparison between the experimental and theoretical hardness of NiCr coatings. Reproduced with permission from Refs. [59,60].

Between the two strengthening mechanisms, grain refinement plays a more significant role in enhancing microhardness. This finding not only provides a solid theoretical foundation but also underscores the practical benefits of incorporating Cr into Ni-based coatings to improve mechanical properties.

5. Conclusions

In this research, by changing the chemical composition, current density and temperature, Ni and NiCr coatings were successfully prepared on 30CrNiMo steel by pulsed current electrodeposition. The microstructure, microhardness, and wear properties of Ni and NiCr coatings were studied. The main results are as follows:

(1) The formic acid and sodium citrate can effectively accelerate the co-deposition of Ni and Cr, facilitating the formation of a NiCr alloy coating on 30CrNiMo steel. Elevating the current density from 200 mA/cm^2 to 300 mA/cm^2 leads to an increase in the Cr content within the NiCr coatings, which varies between 2.6 and 4.4 wt%. The electrodeposited NiCr coatings exhibit a network morphology typical of hard Cr coating, which generate cracks during the electrodeposition due to the formation of chromium hydrides.

(2) The XRD analysis reveals that the NiCr coatings consist of Ni (FCC) single-phase, suggesting the incorporation of Cr element into the NiCr coating as solid solution atoms. Consequently, a Ni-Cr solid solution is established. The grain sizes of the NiCr coatings, as determined by XRD, are approximately 10 nm, 11 nm and 10 nm.

(3) Both Ni and NiCr coatings exhibit significant improvements in wear performance of 30CrNiMo steel substrate. The addition of Cr element further enhances the wear resistance of the coating (Under a normal load of 10 N, the wear rate is reduced from 3.7 $\times$ 10^{-6} to 1.7 $\times$ 10^{-6} mm^3/N·m).

(4) The addition of Cr and grain refinement increases the microhardness of the coatings (from 484 HV to 603 HV). Grain refinement strengthening and solid solution strengthening contributed to the higher hardness of the NiCr coatings compared to Ni coating, and the grain refinement strengthening was mainly strengthening mechanisms.

(5) The NiCr coating is a potential candidate for the brake disc protective coating or replacement for hard chromium coating as far as wear resistance is concerned.

Credit authors statement

Zhan·Liu: Investigation, Methodology, writing-origin-draft, writing-review &editing. Qicheng·Zhang: Investigation, Methodology, writing-origin-draft, writing-review &editing. Xingwen·Zhang: Investigation. Zhifei·Yu: Investigation. Xiaowei·Zhang: Investigation. Qingzhong·Mao: Methodology, writing-origin-draft, writing-review &editing. Jinfeng·Nie: Investigation, Conceptualization, Supervision, Writing-review-&editing. Yonghao·Zhao: Supervision, Funding acquisition, Writing-review-&editing.

Declaration of competing interest

The authors declare that they have no known competing financial interests or personal relationships that could have appeared to influence the work reported in this paper.

Acknowledgement

Y.H. Zhao acknowledges financial supports from the National Key R&D Program of China (Grant No. 2021YFA1200203), National Natural Science Foundation of China (Grant No. 51971112 and 51225102) and Jiangsu Province Leading Edge Technology Basic Research Major Project (BK20222014). J.F. Nie acknowledges financial supports from Natural Science Foundation of Jiangsu Province, China (No. BK20221493). Q.Z. Mao acknowledges financial supports from Jiangsu Funding Program for Excellent Postdoctoral Talent (Grant No. 2023ZB091) and China Postdoctoral Science Foundation (Grant No. 2023M741699). The authors also want to acknowledge the support of the Jiangsu Key Laboratory of Advanced Micro-Nano Materials and Technology. SEM, TEM and EBSD experiments are performed at the Materials Characterization and Research Center of Nanjing University of Science and Technology.

Appendix A. Supplementary data

Supplementary data to this article can be found online at https://doi.

org/10.1016/j.jmrt.2024.04.100.

References

[1] Tsybrii Y, Zglobicka I, Kuciej M, Nosko O, Golak K. Airborne wear particle emission from train brake friction materials with different contents of steel and copper fibres. Wear 2022;504–505:204424.
[2] Yuan B, Liao D, Jiang W, Deng H, Li G, Gu J. Effect of tool tilt angle on microstructure, mechanical properties and fracture behavior of dissimilar friction stir lap welding joint of SiCp/ZL101 and ZL101. J Mater Res Technol 2023;23:4642–62.
[3] Xiang ZY, Zhang JK, Xie SL, Mo JL, Zhu S, Zhai CZ. Friction-induced vibration and noise characteristics, and interface tribological behavior during high-speed train braking: the effect of the residual height of the brake pad friction block. Wear 2023;516–517:204619.
[4] Safavi MS, Bordbar-Khiabani A, Walsh FC, Mozafari M, Khalil-Allafi J. Surface modified NiTi smart biomaterials: surface engineering and biological compatibility. Curr Opin Biomed Eng 2023;25:100429.
[5] Kuptsov KA, Antonyuk MN, Bondarev AV, Sheveyko AN, Shtansky DV. Electrospark deposition of wear and corrosion resistant Ta(Zr)C-(Fe,Mo,Ni) coatings to protect stainless steel from tribocorrosion in seawater. Wear 2021;486–487:204094.
[6] Qin S, Zhang C, Zhang B, Ma H, Zhao M. Effect of carburizing process on high cycle fatigue behavior of 18CrNiMo7-6 steel. J Mater Res Technol 2022;16:1136–49.
[7] Rajaei H, Menapace C, Straffelini G, Gialanella S. Characterization, wear and emission properties of MnS containing laser cladded brake disc. Wear 2022;504–505:204405.
[8] Mozetič M. Surface modification to improve properties of materials. Materials 2019;12:441.
[9] Xia F, Yan P, Ma C, Wang B, Liu Y. Effect of different heat-treated temperatures upon structural and abrasive performance of Ni-TiN composite nanocoatings. J Mater Res Technol 2023;27:2874–81.
[10] Lu C, Li K, Wang C, Li S, Ding J, Jia J, et al. Preparation and tribological properties of NiCr–Mo–Ag–O/Mo–V–Ag–O bilayer film at RT-1000 °C. J Mater Res Technol 2023;26:786–95.
[11] Wang D, Zhao Y, Ge X, Zhang C, Han S, Qiao Z, et al. Designing hard, low-refractive-index lossy materials for super wear-resistant absorbers. Mater Res Lett 2022;10:472–80.
[12] Li Y, Jiang H, Pang L, Wang Ba, Liang X. Novel application of nanocrystalline nickel electrodeposit: making good diamond tools easily, efficiently and economically. Surf Coating Technol 2007;201:5925–30.
[13] Du L, Gao XY, Wang GY, Yang CC, Jiang Q. CeO2 nanoparticles decorated on porous Ni–Fe bimetallic phosphide nanosheets for high-efficient overall water splitting. Mater Res Lett 2023;11:159–67.
[14] Demir M, Kanca E, Karahan İH. Characterization of electrodeposited Ni–Cr/hBN composite coatings. J Alloys Compd 2020;844:155511.
[15] Asghari R, Safavi MS, Khalil-Allafi J. A facile and cost-effective practical approach to develop clinical applications of NiTi: fenton oxidation process. Transactions of the IMF 2020;98:250–7.
[16] Li Y, Cai X, Zhang G, Xu C, Guo W, An M. Optimization of electrodeposition nanocrytalline Ni-Fe alloy coatings for the replacement of Ni coatings. J Alloys Compd 2022;903:163761.
[17] Yao Y, Yao S, Zhang L, Wang H. Electrodeposition and mechanical and corrosion resistance properties of Ni–W/SiC nanocomposite coatings. Mater Lett 2007;61:67–70.
[18] Safavi MS, Fathi M, Ahadzadeh I. Feasible strategies for promoting the mechano-corrosion performance of Ni-Co based coatings: which one is better? Surf Coating Technol 2021;420:127337.
[19] Rasooli A, Safavi MS, Ahmadiyeh S, Jalali A. Evaluation of TiO2 nanoparticles concentration and applied current density role in determination of microstructural, mechanical, and corrosion properties of Ni–Co alloy coatings. Protect Met Phys Chem Surface 2020;56:320–7.
[20] Kong X, Liu Y, Chen M, Zhang T, Wang Q, Wang F. Heterostructured NiCr matrix composites with high strength and wear resistance. J Mater Sci Technol 2022;105:142–52.
[21] Sidhu TS, Prakash S, Agrawal RD. Hot corrosion performance of a NiCr coated Ni-based alloy. Scripta Mater 2006;55:179–82.
[22] Romedenne M, Haynes A, Pillai R. Cyclic oxidation behavior of selected commercial NiCr-alloys for engine exhaust valves in wet air environment between 800 and 950 °C. Corrosion Sci 2023;211:110817.
[23] Kang JC, Lalvani SB, Melendres CA. Electrodeposition and characterization of amorphous Fe-Ni-Cr-based alloys. J Appl Electrochem 1995;25:376–83.
[24] Zhou Y, Zhao G, Zhang H. Fabrication and wear properties of co-deposited Ni-Cr nanocomposite coatings. Trans Nonferrous Metals Soc China 2010;20:104–9.
[25] Lin K, Ho J. Electrodeposited Ni-Cr and Ni-Cr-P alloys. J Electrochem Soc 1992;139:1305.
[26] Liu S, Shohji I, Kobayashi T, Hirohashi J, Wake T, Yamamoto H, et al. Mechanistic study of Ni–Cr–P alloy electrodeposition and characterization of deposits. J Electroanal Chem 2021;897:115582.
[27] Gupta VK, Shrivastava AK, Jain N. Biosorption of Chromium(VI) from Aqueous solutions by green algae spirogyra species. Water Res 2001;35:4079–85.
[28] Mohanty S, Benya A, Hota S, Kumar MS, Singh S. Eco-toxicity of hexavalent chromium and its adverse impact on environment and human health in Sukinda Valley of India: a review on pollution and prevention strategies. Environ Chem Ecotoxicol 2023;5:46–54.
[29] Tharamani CN, Hoor FS, Begum NS, Mayanna SM. Electrodeposition and characterization of Ni–Cr alloy coating. J Electrochem Soc 2006;153:C164.
[30] Thakur A, Gangopadhyay S. State-of-the-art in surface integrity in machining of nickel-based super alloys. Int J Mach Tool Manufact 2016;100:25–54.
[31] Singh A, Ghosh S, Aravindan S. State of art for sustainable machining of nickel-based alloys using coated and uncoated tools and machining of high strength materials using surface modified cutting tools. Tribol Int 2022;170:107517.
[32] Liang A, Ni L, Liu Q, Zhang J. Structure characterization and tribological properties of thick chromium coating electrodeposited from a Cr(III) electrolyte. Surf Coating Technol 2013;218:23–9.
[33] Jeyaraj S, Arulshri KP, Ramesh S, Muthukumaran G. Experimental investigations and effects studies on electrodeposited Ni-Cr composite coating using robust design approach. Mater Today Proc 2018;5:6999–7008.
[34] Zhu Y, Gu C-Q, Wang J, Xi X, Qin Z. Characterization and corrosion behavior of Ni-Cr coatings by using pulse current electrodeposition. Anti-corrosion Methods & Mater 2023;70:236–42.
[35] Xu L-j, Gong Z-q, Tang J-x, He Q-g, He N-y, Du J-j. Ni-Cr alloy electrodepositing technology on Fe substrate and coating performance. J Cent S Univ Technol 2007;14:181–5.
[36] Sheibani Aghdam A, Allahkaram SR, Mahdavi S. Corrosion and tribological behavior of Ni–Cr alloy coatings electrodeposited on low carbon steel in Cr (III)–Ni (II) bath. Surf Coating Technol 2015;281:144–9.
[37] Survilienė S, Češūnienė A, Jasulaitienė V, Jurevičiūtė I. The use of XPS for study of the surface layers of CrNi alloys electrodeposited from the Cr(III)+Ni(II) bath. Appl Surf Sci 2012;258:9902–6.
[38] Giovanardi R, Orlando G. Chromium electrodeposition from Cr(III) aqueous solutions. Surf Coating Technol 2011;205:3947–55.
[39] Bojinov M, Fabricius G, Kinnunen P, Laitinen T, Mäkelä K, Saario T, et al. Electrochemical study of the passive behaviour of Ni–Cr alloys in a borate solution—a mixed-conduction model approach. J Electroanal Chem 2001;504:29–44.
[40] Zhang P, Zou L, Wang X. Ni-Cr alloy electrodeposition. Mater Prot 1997;30:16–8.
[41] Zhang P, Zou L, Wang X. Influencing factors on Cr content in Ni-Cr deposit. Mater Prot 1997;30:22–3.
[42] Chen L, Cong Z, Huang Z, Tu F, Jiang H. Study of nickel-chromium electrodeposit. Plating and Finish 1998;17:4–7.
[43] Yang Y, Gong Z, Deng L, Luo B, Ma Y, Yang Z. Electrodeposition of Ni-Cr alloy on aluminum substrate. J Cent S Univ Technol 2006;13.
[44] Zhang H, Liu L, Bai J, Liu X. Corrosion behavior and microstructure of electrodeposited nano-layered Ni–Cr coatings. Thin Solid Films 2015;595:36–40.
[45] Huang CA, Lin CK, Chen CY. Hardness variation and corrosion behavior of as-plated and annealed Cr–Ni alloy deposits electroplated in a trivalent chromium-based bath. Surf Coating Technol 2009;203:3686–91.
[46] Tang PT. Pulse reversal plating of nickel and nickel alloys for microgalvanics. Electrochim Acta 2001;47:61–6.
[47] Firouzi-Nerbin H, Nasirpouri F, Moslehifard E. Pulse electrodeposition and corrosion properties of nanocrystalline nickel-chromium alloy coatings on copper substrate. J Alloys Compd 2020;822:153712.
[48] Haché MJR, Zou Y, Erb U. Post-deposition crack evolution in Cr(III) alloy electrodeposits: phenomenology. Surf Coating Technol 2021;406:126648.
[49] Lausmann GA. Electrolytically deposited hardchrome. Surf Coating Technol 1996;86–87:814–20.
[50] Lim D, Ku B, Seo D, Lim C, Oh E, Shim SE, et al. Pulse-reverse electroplating of chromium from Sargent baths: influence of anodic time on physical and electrochemical properties of electroplated Cr. Int J Refract Metals Hard Mater 2020;89:105213.
[51] Imaz N, Ostra M, Vidal M, Díez JA, Sarret M, García-Lecina E. Corrosion behaviour of chromium coatings obtained by direct and reverse pulse plating electrodeposition in NaCl aqueous solution. Corrosion Sci 2014;78:251–9.
[52] Karmazin L. Lattice parameter studies of structure changes of Ni-Cr alloys in the region of Ni2Cr. Mater Sci Eng 1982;54:247–56.
[53] Etminanfar MR, Heydarzadeh Sohi M. Corrosion resistance of multilayer coatings of nanolayered Cr/Ni electrodeposited from Cr(III)–Ni(II) bath. Thin Solid Films 2012;520:5322–7.
[54] Patterson AL. The scherrer formula for X-ray particle size determination. Phys Rev 1939;56:978–82.
[55] Sun X, Fan Y, Nie J, Chen Y, Xie K, Liu S, et al. Significant improvement of the room and cryogenic mechanical properties of an AlN particle reinforced Al matrix composite by alloying element magnesium. Compos B Eng 2024;268:111056.
[56] Kong J, Haché MJR, Tam J, McCrea JL, Howe J, Erb U. On the extrinsic Hall-Petch to inverse Hall-Petch transition in nanocrystalline Ni-Co electrodeposits. Scripta Mater 2022;218:114799.
[57] Matsui I, Uesugi T, Takigawa Y, Higashi K. Effect of interstitial carbon on the mechanical properties of electrodeposited bulk nanocrystalline Ni. Acta Mater 2013;61:3360–9.
[58] Liu P, Yuan X, Du Y, Long M, Duan H, Chen D. Exploration of electrodeposited process of Ni-Co-Cr coating and investigation of Cr doping strengthening mechanism by indentation simulation. J Mater Process Technol 2023;311:117818.
[59] Schuh CA, Nieh TG, Yamasaki T. Hall–Petch breakdown manifested in abrasive wear resistance of nanocrystalline nickel. Scripta Mater 2002;46:735–40.
[60] Ibáñez A, Escudero-Cid R, Ocón P, Fatás E. Effect of the pulse plating parameters on the mechanical properties of nickel electrodeposits. Surf Coating Technol 2012;212:94–100.